FORSCHUNGSZENTRUM JÜLICH GmbH

Institut für Plasmaphysik
Association EURATOM-KFA

Asymmetry of Radial Heat Pulse Propagation at TEXTOR

A. Krämer-Flecken A. Rogister M.Z. Tokar'
G. Waidmann G.H. Wolf

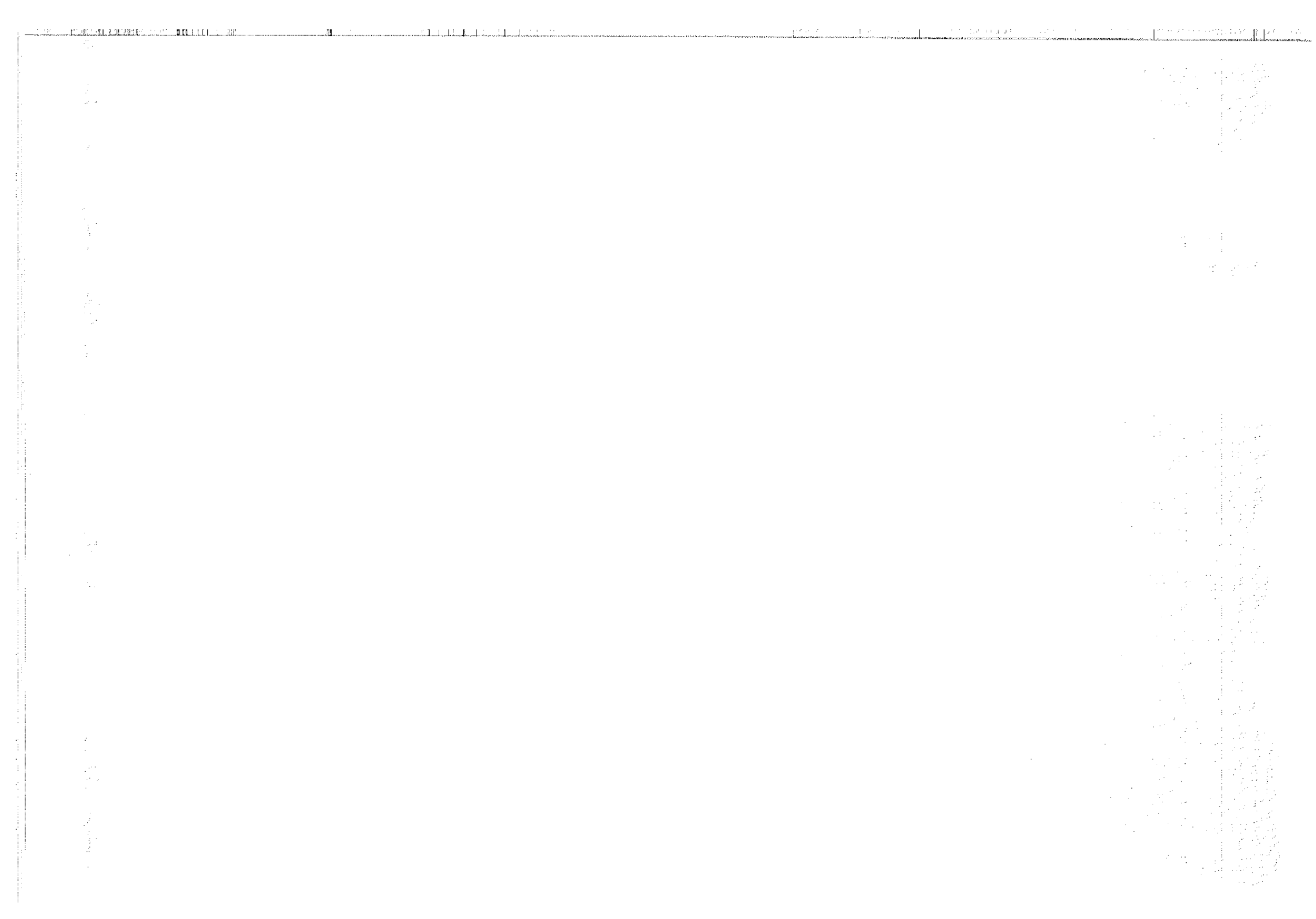

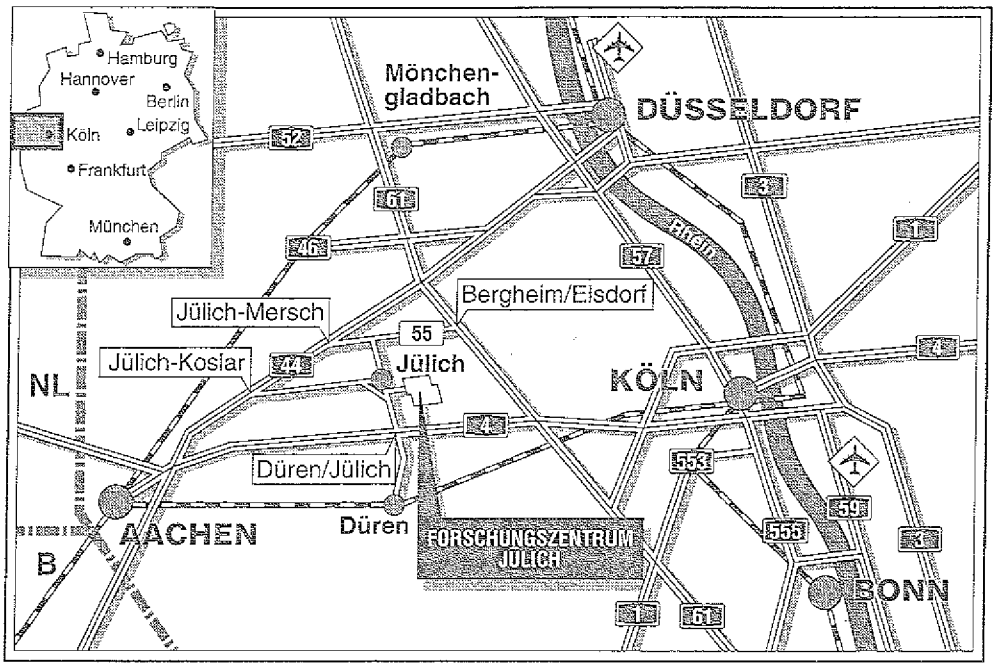

Berichte des Forschungszentrums Jülich ; 2680
ISSN 0366-0885
Institut für Plasmaphysik Jül-2680
Association EURATOM-KFA

Zu beziehen durch: Forschungszentrum Jülich GmbH · Zentralbibliothek
Postfach 1913 · D-5170 Jülich · Bundesrepublik Deutschland
Telefon: 02461/61-6102 · Telefax: 02461/61-6103 · Telex: 833556-70 kfa d

Asymmetry of Radial Heat Pulse Propagation at TEXTOR

A. Krämer-Flecken A. Rogister M.Z. Tokar'*
G. Waidmann G.H. Wolf

*supported by the A.v.Humbold foundation
permanent address: Institute for High Temperatures, Moscow, Russia

Abstract

Electron heat pulse propagation following sawtooth collapse has been simultaneously observed along two opposite radial directions. For a given flux surface the arrival of the heat pulse at the high field side (HFS) is delayed by up to 1ms as compared to the arrival at the low field side (LFS). The observed delay agrees with an estimate of the time required for parallel electron heat transport along the magnetic field lines connecting the corresponding LFS and HFS isobars. This suggests that the primary radial heat transport occurs on the LFS, whereas the HFS is fed subsequently from the LFS by temperature equilibration along the connecting magnetic field lines.

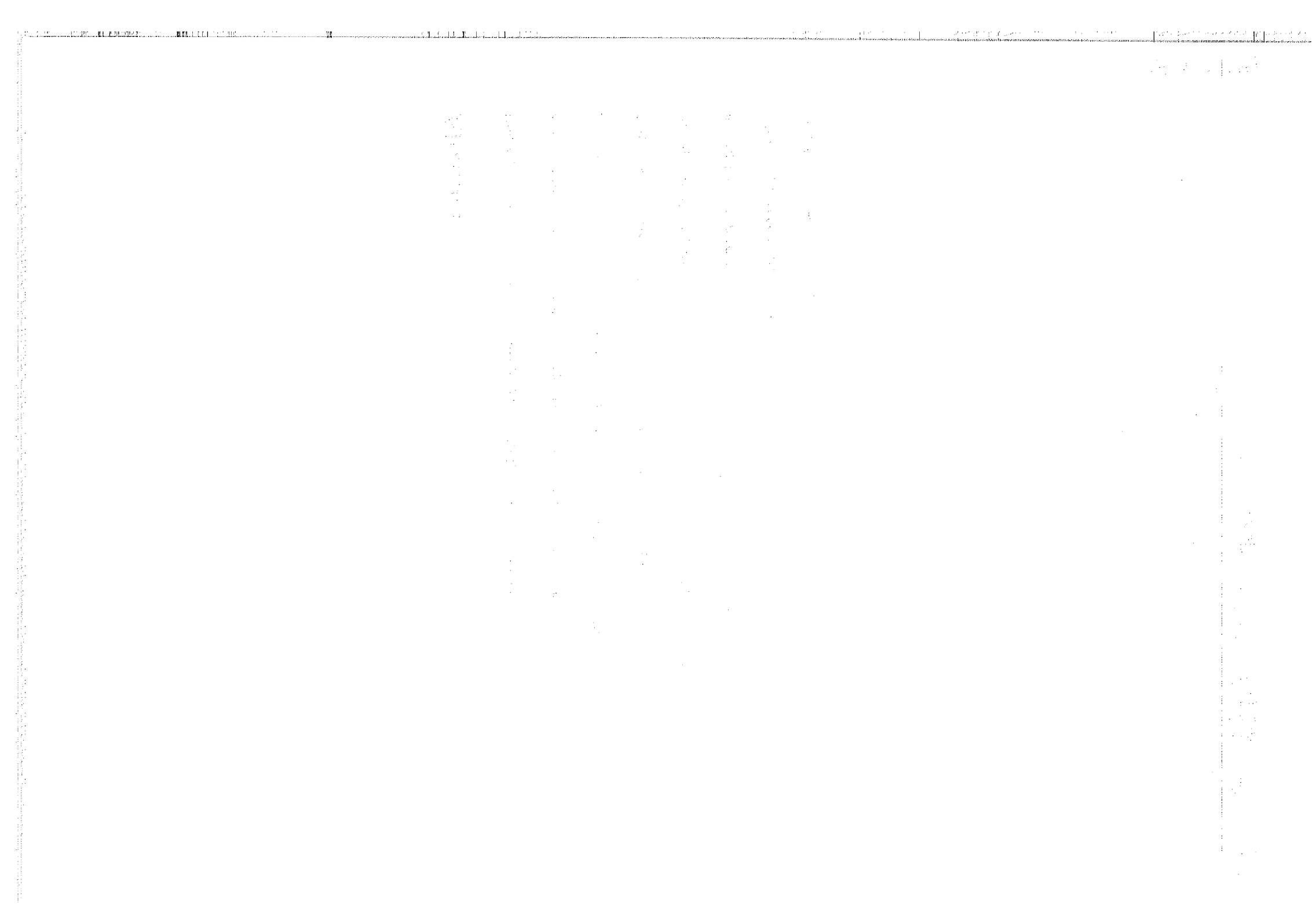

1. Introduction

It is usually assumed that electron heat transport is governed by a diffusive process across the entire magnetic surface, and consequently that $\chi_e(r)$ is a useful characteristic quantity to describe this process. Experimentally $\chi_e(r)$ is commonly derived from the (quasi-)stationary energy balance[1]. Complementing this standard procedure, perturbation methods have been applied to calculate the χ_e-values from the radial propagation of transients on the T_e- and n_e-profiles[2,3]. An intrinsic source of such transients is the sawtooth collapse occurring in tokamaks under many discharge conditions.

Previous analyses of the heat pulse propagation following the sawtooth collapse were based on observations along one radial direction only, except recently[6]. They addressed the question whether, and to which extent, the χ_e-values derived from heat pulse propagation differ from those obtained from the stationary power balance.

The present paper reports on the simultaneous observation of heat pulse propagation along two radial directions in the equatorial plane, i.e. along both the high field side (HFS) and the low field side (LFS). The measured delay between the arrival of the heat pulses on the same magnetic surface leads to the conclusion that the observed pattern, initiated by an asymmetric sawtooth crash, can be only explained by the combined action of parallel and perpendicular transport.

2. The experimental set-up

At TEXTOR ($B_T = 2.25T$ at $R_0 = 1.75m$, $a = 0.46m$) a heterodyne ECE-diagnostic[4] had been installed to measure the electron temperature on the equatorial plane at 10 different radial positions. The radiometer frequencies are radially placed from 105 GHz to 145 GHz in steps of 5 GHz. The spatial resolution of each system is $\Delta R = \pm 0.7cm$ and the data sampling rate is 10 kHz. On both the LFS and the HFS a tuneable radiometer is available, covering a frequency range of $137 \leq f \leq 150$ GHz on the HFS and $102 \leq f \leq 113$ GHz on the LFS. To measure the electron temperature dynamics in steps of 1 GHz, 15 reproducible discharges were necessary.

A multichannel HCN-interferometer[5] positioned 180° toroidally apart from the ECE-system yielded information on the electron density profiles and on the temporal development of the local electron density during the sawtooth collapse. Three interferometer channels on the HFS and four interferometer channels on the LFS are placed in the region which is covered by the tuneable radiometers.

The radial temperature and density development was measured for two series of ohmically heated plasmas with the following plasma parameters: $Ip = 350KA$, $\bar{n}e = 2.1 * 10^{13} cm^{-3}$ and $B_T = 2.25$ respectively $B_T = 2.22T$. The Z_{eff}-values for carbon were measured to $Z_{eff} = 1.5$ for the first series ($B_T = 2.25T$) and $Z_{eff} = 2.0$ for the second one ($B_T = 2.22T$). In order to increase the statistical accuracy a time interval from $0.5 \leq t \leq 1.2s$ was analyzed containing around 40 individual sawtooth events for each discharge.

3. Experimental Results

3.1 Heat pulse propagation time

The heat pulse propagation analysis is confined to an area outside the sawtooth inversion radius. The heat pulse propagation time is defined as the time at which the temperature maximum (maximum amplitude) of the heat pulse reaches a certain radial position $R_0 \pm r$, after a sawtooth crash in the plasma center.

The raw data were covered with statistical noise and contributions from plasma fluctuations. Since the sawtooth period of $\tau = 16.0$ms (respectively $\tau = 12.8$ms for the second series) was stable within 5%, a Fourier analysis could be used to suppress the noise. From the first 4 harmonics of the sawtooth period, the heat pulse propagation time t_p was obtained for the different radial positions.

For both discharge series the general behaviour of the heat pulse propagation was found to be similar on the HFS and on the LFS. As a general feature, the velocity of the radial heat pulse propagation decreased with increasing radial distance from the origin of the collapse. From the radial dependence of the heat pulse propagation time we deduced a velocity of $v = 35$m/s at $|R-R_0|/a = 0.55$ on the HFS and of $v = 34$m/s at $|R-R_0|/a = 0.84$ on the LFS for $B_T = 2.25$T. For the discharge series with $B_T = 2.22$T, the same analysis yields velocities of $v = 33$m/s at $|R-R_0|/a = 0.63$ on the HFS and $v = 29$m/s at $|R-R_0|/a = 0.75$ on the LFS.

3.2 Evolution of T_e-Profiles during sawtooth crash

The electron temperature profiles were obtained from coherently averaged ECE-data. During the investigated time interval, around 40 sawtooth periods were overlaid, taking the sawtooth crash in the plasma center, (defined by the largest temperature variation), as starting signal.

For both discharge series the inversion radius, deduced from the T_e-profiles, was about $r_{INV} \approx 10$cm. Precursor activity just before the sawtooth crash occurred with a frequency of about 3.3kHz corresponding to an oscillation period of $\tau = 300\mu s$.

At the toroidal position of the ECE-diagnostic the starting position of the sawtooth crash was always localized on the LFS[6]. From there the crash moved within about $200\mu s$ towards the HFS, i.e. during a time which corresponds to half of the precursor period. Looking for temperature changes, by subtracting subsequent T_e-profiles during the onset phase of the sawtooth crash from each other, the LFS exhibits a radial region where the temperature increases, i.e. a region of inverted sawtooth, whereas no indications for such an inverted region were found on the HFS (fig 1). However, subtracting the T_e-profiles just before the sawtooth crash from those taken $300\mu s$ later shows a region of inverted sawteeth on both the HFS and the LFS. Moreover, comparing both curves shows that the (radial) position of the maximum temperature amplitude in the center has moved slightly towards the HFS, as indicated by the arrows in fig. 1.

Both the sawtooth crash dynamics as well as the early state of the heat pulse development become also visible from a T_e-contour plot of the averaged ECE-data

covering the vicinity of the sawtooth crash (fig. 2). There a pronounced spike on the LFS-isotherm develops during the sawtooth crash (A) indicating the plasma outflow from a hot spot localized on the LFS[7]. This spike disturb the isotherms up to $r \approx 24$cm on the LFS, whereas on the HFS no indication of an equivalent process was found but rather a common shift, of the isotherms with $T_e \geq 900$eV, toward the LFS. First indications for the occurrence of the heat pulse on the HFS were observed on the $T_e = 850$eV isotherm (B) about $\Delta t \approx 200\mu$s after the sawtooth crash. If the hot spot is subject of a poloidal rotation, i.e. of an $m = 1$, $n = 1$ mode structure, and by accounting for the precursor period of 300μs, an outflow of hot plasma on the HFS should occur about 200μs after the onset of the sawtooth crash on the LFS. However, since no indication of such an outflow of the hot plasma towards the HFS could be found, the release of the hot plasma is assumed to occur only on the LFS.

An opposite event was found when analyzing the n_e-profiles. The n_e-diagnostic, 180° toroidally apart from the T_e-diagnostic, shows the beginning of the sawtooth crash on the HFS. This behaviour suggests a correlation between the precursor activity and the sawtooth crash[8]. Furthermore, the combined results of both diagnostics support the assumption of a $m = 1, n = 1$ mode structure existing before the sawtooth crash.

From the asymmetry in the sawtooth crash an initial time delay between HFS and LFS is expected. Comparing the inverted T_e-sawtooth-signal outside the inversion radius we found a time offset of $\Delta t \sim 400\mu$s between the radiometer EC6 on the HFS located at $R\text{-}R_0 = -11.2$cm and a radial position at $R\text{-}R_0 = 19.9$cm on the LFS (fig. 3). Both positions correspond to the same original isobar.

4. Interpretation of the data

4.1 Heat pulse propagation on isobars

For a comparison of the heat pulse propagation on the LFS and HFS, a transformation into the coordinate system of the (unperturbed, original) flux surfaces, assumed to be characterized by isobars, is necessary. In order to obtain the corresponding pressure profiles, the HCN-data were also coherently averaged, using the sawtooth crash in the plasma center as trigger signal. The resulting density profile, averaged over the precursor activity before the crash, was multiplied with the temperature profile (taken in the same time interval as the density profile). This procedure yields the "unperturbed" p_e-profile and its shift with respect to the geometrical axis $R_0 = 1.75$m. To make sure that the influence of the sawtooth crash on the so obtained reference isobars is small, the p_e-profile after the sawtooth crash was also calculated: The isobar radii deduced from these two profiles coincide in the relevant radial range of $16 \leq r_{fs} \leq 35$cm within a margin of $0.1 \leq \Delta r \leq 0.3$cm. Plotting the heat pulse propagation time as a function of the isobar radius (fig. 4) exhibits a distinct difference in the propagation time between the HFS and LFS. In both series, at the toroidal position of the ECE-diagnostic, the heat pulse propagation is significantly faster on the LFS than on the HFS. Already during the initial development of the heat pulse occurring just outside of the inversion radius such a temporal asymmetry was found, which is the result of the preceding process as described in section 3.2 and fig. 1. The observed

deviations fall outside any uncertainty in the relative isobaric position before and after the sawtooth crash. In fact, to obtain fictitiously an equal propagation time along both directions, an inward shift of the whole plasma column of more than 2cm would be required during the heat pulse propagation phase. These results remain essentially the same if, instead of the p_e-profile, the n_e-profile or T_e-profile was taken as reference frame.

In fig. 4a the error bars of the heat pulse propagation time overlap in some cases, but a systematic time difference Δt_p between LFS and HFS is visible, which increases with the isobar radius. In Fig. 4b this time difference becomes even more pronounced. For an isobar radius of 30cm Δt reached values of up to $\Delta t \approx 1$ms.

Furthermore, we performed a discharge series ($I_p = 350$KA, $B_T = 2.25$T and $\bar{n}_e = 2.5 * 10^{13} cm^{-3}$) where the horizontal position of the density peak was changed from $R\text{-}R_0 = -0.7$cm to $R\text{-}R_0 = 8.0$cm, with fixed radiometer frequency settings. Also in this case, the analysis showed a much faster radial heat pulse propagation on the LFS than on the HFS (fig 5).

In view of the observed difference in the heat pulse propagation between the HFS and the LFS, the question arises whether there is also some difference in the amplitudes of the inverted sawteeth on the HFS and the LFS for corresponding isobar radii. The amplitude development of the inverted sawtooth versus isobar radius is shown in fig. 6. For $r_{fs} \leq 24$cm a strong difference was indeed found between HFS and LFS. At the beginning of the observation interval the measured amplitude on the LFS is nearly twice as high as on the HFS. For $r_{fs} \geq 25$cm, however, the measurement of the amplitudes become perturbed by noise and the difference in amplitudes between LFS and HFS diminished. Furthermore, the

density perturbation caused by the sawtooth crash had vanished at $r_{fs} \approx 25$cm.

Both observations, the asymmetric heat pulse propagation as well as the asymmetric development of the inverted sawtooth amplitude do not appear to be compatible with the concept of a predominantly diffusive process across the entire magnetic surface. Instead, they indicate the dominance of a rather localized primary radial heat transport mechanism at the LFS, whereas in a subsequent process the heat is transported from the LFS to the HFS along the connecting field lines via parallel heat conduction. The isotherm pattern as shown in fig. 2 reveals this impression in a suggestive manner. This is in analogy to the flow of water forced to pulsate in an axisymmetric cascade fountain which consists of superimposed concentric circular basins that are, however, not properly aligned in the horizontal plane but slightly tilted to one side.

Considering the whole toroidal circumference we assume that the radial heat pulse is launched from a helical starting position. This is in accord with the observation of the HCN-interferometer[8].

4.2 Estimate of parallel heat propagation

In order to test the consistency of the proposed transport model, the electron heat transfer time between LFS and HFS along the connecting magnetic field line has to be estimated. Two approximations on this question were performed.

In the first approach we analyze at first the ratio between the connection length L_c for the transport along the magnetic field B (coordinate l) between the LFS and HFS and the path length λ_c between Coulomb collisions. Considering a magnetic

surface with a value of $q \approx 2$ we obtain $L_c = \pi \cdot q \cdot R_0$, i.e. (for $R_0 = 1.75$ m) $L_c \approx 11$m. By comparison, an estimate of $\lambda_c \approx 10^{10} T_e^2/n_e$ (m, eV, cm^{-3}) yields values in the range of 8-180m, since $100eV \leq T_e \leq 650eV$ and $1.3 \times 10^{13} cm^{-3} \leq n_e\ 2.3 \times 10^{13} cm^{-3}$ are the relevant plasma parameters in the interesting radial region. Therefore the electron heat propagation from the LFS to the HFS is of a collisionless nature, associated with the motion of particles under the influence of an electric field $E_\parallel$ which is caused by the different behaviour of electrons and ions. Since the electrons acquire a near Boltzmann distribution rather quickly, the electron pressure gradient caused by the temperature perturbation is balanced by the resulting electric force

$$\partial(T_e \cdot n_e)/\partial l = -e \cdot n_e \cdot E_\parallel \qquad (1)$$

The deviation from an exact Boltzmann distribution results from an acceleration of the ions in this electric field towards the LFS

$$m_i \cdot \frac{dV_\parallel}{dt} = e \cdot E_\parallel \qquad (2)$$

which then leads in a quasi-neutral plasma to a net motion of the electrons with the same velocity $V_\parallel$.

From eqs. (1) and (2) we obtain the following estimates for the characteristic values of the velocity $V_\parallel$ and of the time $\tau_D \approx L_s/V_\parallel$ characterizing the electron heat propagation from the LFS to the HFS:

$$V_{\parallel} \simeq \sqrt{\Delta T_e / m_i} \tag{3}$$

$$\tau_D \simeq \frac{\pi \cdot q \cdot R}{\sqrt{\Delta T_e / m_i}} \tag{4}$$

Taking the largest observed difference between the T_e-perturbations on the HFS and LFS on the same isobar and taking q-values derived from standard current profile[9], equ.(4) shows an increase in τ_D with decreasing ΔT_e, yielding $\tau_T = 0.39$ms at a flux surface radius of $r_{fs} = 24.0$cm and $\tau_D = 0.83$ms at $r_{fs} = 30.5$cm.

The second approach starts from the assumption that the original heat puff is expelled at the time $t = t_1$ across the neutral (X)-line of the equation $\varphi = \vartheta$, $r = r_1$[10]. This concept is supported by the TEXTOR density and electron temperature diagnostics[8]. Again, the delay time of the perturbation between the LFS and HFS isobars, depends on the decay rate of ion sound waves. From the linearized one-dimensional Vlasov equation it is shown that the dispersion relation of modes with frequency ω and parallel wave vector $k_{\parallel}$ is

$$\sum_j (e_j^2 / m_j) \int dv_{\parallel} (\omega - k_{\parallel} \cdot v_{\parallel})^{-1} k_{\parallel} \partial F_s / \partial v_{\parallel} = 0 \tag{5}$$

where the summation is over the particle species and the integrals are along the Landau contour. We expand the propagator in the way usual for sound waves, i.e. $v_{\parallel,i} << |\omega/k_{\parallel}| << v_{\parallel,e}$, consider Maxwellian electron and ion backgrounds, and evaluate accordingly the Cauchy principal parts and the residues of the integrals. This yields the approximate Re $\omega = \pm k_{\parallel} c_s$ solution, where $c_s = (T_e/m_i)^{1/2}$ is the "sound speed" and

$$\gamma = Im\omega = -\frac{1}{2}\left(\frac{\pi}{2}\right)^{1/2}\left[\left(\frac{T_e}{T_i}\right)^{3/2}\exp(-T_e/2T_i) + \left(\frac{m_e}{m_i}\right)^{1/2}\right]|k_\parallel| c_s \qquad (6)$$

To estimate a characteristic length, we introduce the angular coordinates $\Phi = 0$ or 2π and $\Theta = \pi$ of the inboard detection position in the equation $\Phi - \varphi_0 = q(\Theta - \vartheta_0)$ of a field line crossing the line $\varphi = 0$ of a pitch unity at $\varphi_0 = \vartheta_0$. We obtain $\vartheta_0 = q\pi/(q-1)$ or $(q-2)\pi/(q-1)$ and, accordingly, $\Phi - \varphi_0 = \pm\, q\pi/(q-1)$. The required length is therefore $L_\parallel = [R^2(\Phi-\varphi_0)^2 + r^2(\Theta-\vartheta_0)^2]^{1/2} \sim \pi qR/(q-1)$. Thus, from equ. 6, the time delay between the signal on the corresponding HFS and LFS isobar should be

$$\tau_D(ms) \sim 0.045\cdot[A_i/T_e(KeV)]^{1/2}\cdot q/(q-1) \qquad (7)$$

where A_i is the ion atomic mass. Taking $R = 1.75$m and introducing again $T_e = T_i = 0.1$KeV and $q = 2$, we obtain for τ_D a value of $\tau_D = 0.4$ms. Since closer to the plasma edge one observes that $T_e < T_i$, a situation that corresponds to a smaller Landau damping rate, we may take $T_i = 2T_e$. Then, again for $T_e = 0.1$KeV and $q = 2$ one obtains $\tau_D = 0.8$ms. The use of the exact plasma dispersion function instead of the approximations which leads to equ. (7) modifies the results by less than 15%.

The τ_D values obtained from the above estimates are in acceptable agreement with the observed delay time of the heat pulse propagation, thus supporting our proposed model.

5. Conclusion

Using an ECE-diagnostic array located in a certain toroidal position, the radial

propagation of the electron heat pulse following sawtooth crashes was measured simultaneously on both the LFS and the HFS. The heat pulse propagation time was analyzed with respect to the corresponding isobars on the LFS and HFS, deduced from the unperturbed original p_e-profile. Systematically, the arrival of the heat pulse on the LFS isobar occurred (up to 1ms) earlier than on the corresponding HFS isobar. The difference in the arrival time increases with the isobar radius. This asymmetry of the local heat pulse propagation was initiated by a hot spot - (best observed on the T_e-contour plots) - releasing the "high temperature content" on the LFS.

These observations suggest that the primary and predominant radial electron heat transport is localized on the LFS and that the HFS is only fed subsequently by parallel heat equilibration along the connecting magnetic field lines. An estimate of the time delay τ_D necessary for parallel heat equilibration between HFS and LFS is in satisfactory agreement with these experimental results. The proposed explanation of the observed transport pattern, i.e. competing participation of both, perpendicular and parallel electron heat transport, is also supported by the measured asymmetry in the amplitudes of the heat pulses between LFS (larger amplitude) and HFS (smaller amplitude).

Altogether, these results challenge the concept of a homogeneous, simultaneous diffusive transport across the magnetic surfaces. Instead, for a quantitative analysis of the electron heat transport coefficients, a three dimensional treatment is required.

Acknowlegdment

The authors wish to thank the TEXTOR team for operating the machine and they wish to express their appreciation to Dr. Kever for helpful suggestions during many discussions.

References

[1] Tubbing, B.J.D., Lopez Cardozo, N.J., Van der Wiel, M.J., Nucl. Fusion 27 (1987) 1843

[2] Jahns, G.L., Soler, M., Waddell, B.V., Callen, J.D., Hicks, H.R., Nucl. Fusion 18 (1978) 609

[3] Lopez Cardozo, N.J., Tubbing, B.J.D., Tibone, F., Taroni, A., Nucl. Fusion 28 (1988) 1173

[4] Waidmann, G., Cao, Y., Jadoul, M., Kardon, B., EC-7 Workshop on ECE and ECRH, Hefei, China, 1989, p. 92-99

[5] Soltwisch, H., Rev. Sci. Instrum., 57, (1986) 1939

[6] Fredrickson, E.D., McGuire, K., Cavallo, A., et al., Phys. Rev. Lett. Vol 65, No. 23, (1990) 2869

[7] Park, W., Monticello, D.A., Fredrickson, E., McGuire, K., Phys. Fluids B 3 (3) (1991), 507

[8] Koslowski, H. R., Krämer-Flecken, A., in *Proceedings of the 19th European Conference on Controlled Fusion and Plasma Physics Innsbruck 1992* Vol.1 p. 383

[9] Soltwisch, H., Messung der internen Magnetfeld-Struktur von Tokamak-Plasmen, Jül - 2339, Forschungszentrum Jülich, 1990

[10] Rogister, A., Hasselberg, G., Li, D., Psimopoulos, M., Soltwisch., H., in *Proceedings of the 13th International Conference on Plasma Physics and Controlled Fusion 1990, Washington, D.C.* (IAEA, Vienna, 1991) Vol. 2 p. 231

Figure 1: Temperature difference $\Delta T_e(r)$ deduced from two T_e-profiles in the beginning of the sawtooth crash $\Delta t = 100\mu s$ (curve 1). Curve 2 displays $\Delta T_e(r)$ for subtracting a T_e-profile after the sawtooth crash from one in the onset of the crash ($\Delta t = 300\mu s$). The arrows mark the position of the crash center.

Figure 2: T_e-contour plot displaying the sawtooth crash and the release of the plasma on the LFS and the delay between the occurrence of the inverted sawtooth on the LFS and the HFS. The isotherms up to $T_e = 1000eV$ are plotted in steps of 100eV. For $T_e > 1000eV$ in steps of 50eV.

A: Indicates the spike on the isotherms on the LFS

B: Indicates the first occurrence of an inverted sawtooth on the HFS

Figure 3: Comparision of the inverted sawtooth on the same isobar ($r_{fs} = 15.6cm$) for both LFS and HFS. The amplitude of the LFS sawtooth is reduced by a factor 0.73 for better comparision. The time offset between LFS and HFS of about $400\mu s$ is clearly seen.

Figure 4: Heat pulse propagation time versus isobar radius for the two series. Both display a time offset between LFS and HFS and a much faster heat pulse propagtion on the LFS. Plasma parameters: (a) $I_p = 350kA$, $B_T = 2.25T$, $\bar{n}_e = 2.1 * 10^{13} cm^{-3}$, $Z_{eff} = 1.5$; (b) $I_p = 350kA$, $B_T = 2.22T$, $\bar{n}_e = 2.1 * 10^{13} cm^{-3}$, $Z_{eff} = 2.0$;

Figure 5: Heat pulse propagation time versus isobar radius (observed by shifting the horizontal plasma position).

Figure 6: Asymmetric development of the inverted sawtooth amplitude plotted versus isobar radius. The amplitude of LFS and HFS become equal for a radius $r_{fs} \geq 25cm$.

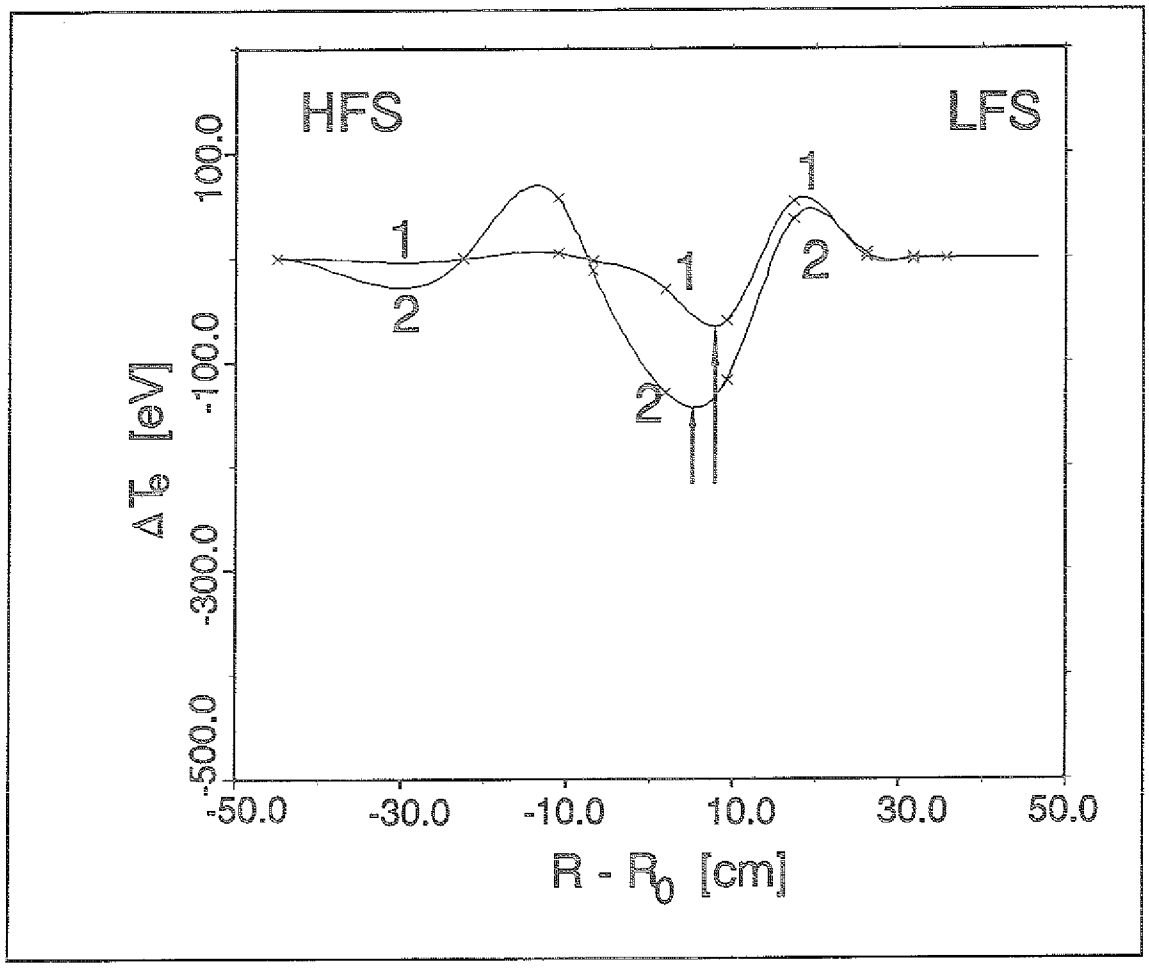
HFS
LFS
100.0
-100.0
-300.0
-500.0
ΔTe [eV]
-50.0
-30.0
-10.0
10.0
30.0
50.0
R - R0 [cm]
1
2
1
2
1
2

Figure 1

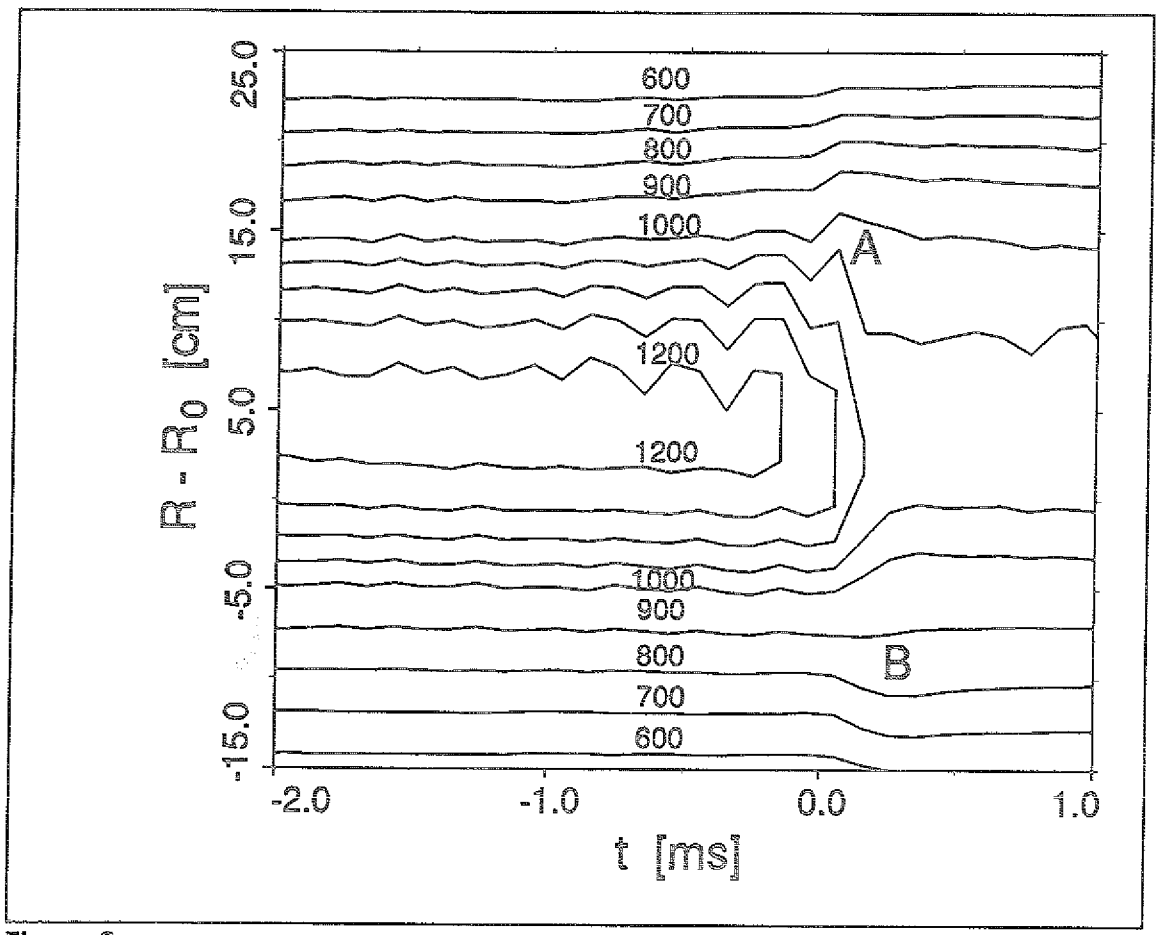
25.0
15.0
5.0
-5.0
-15.0
R - R0 [cm]
600
700
800
900
1000
A
1200
1200
1000
900
800
B
700
600
-2.0
-1.0
0.0
1.0
t [ms]

Figure 2

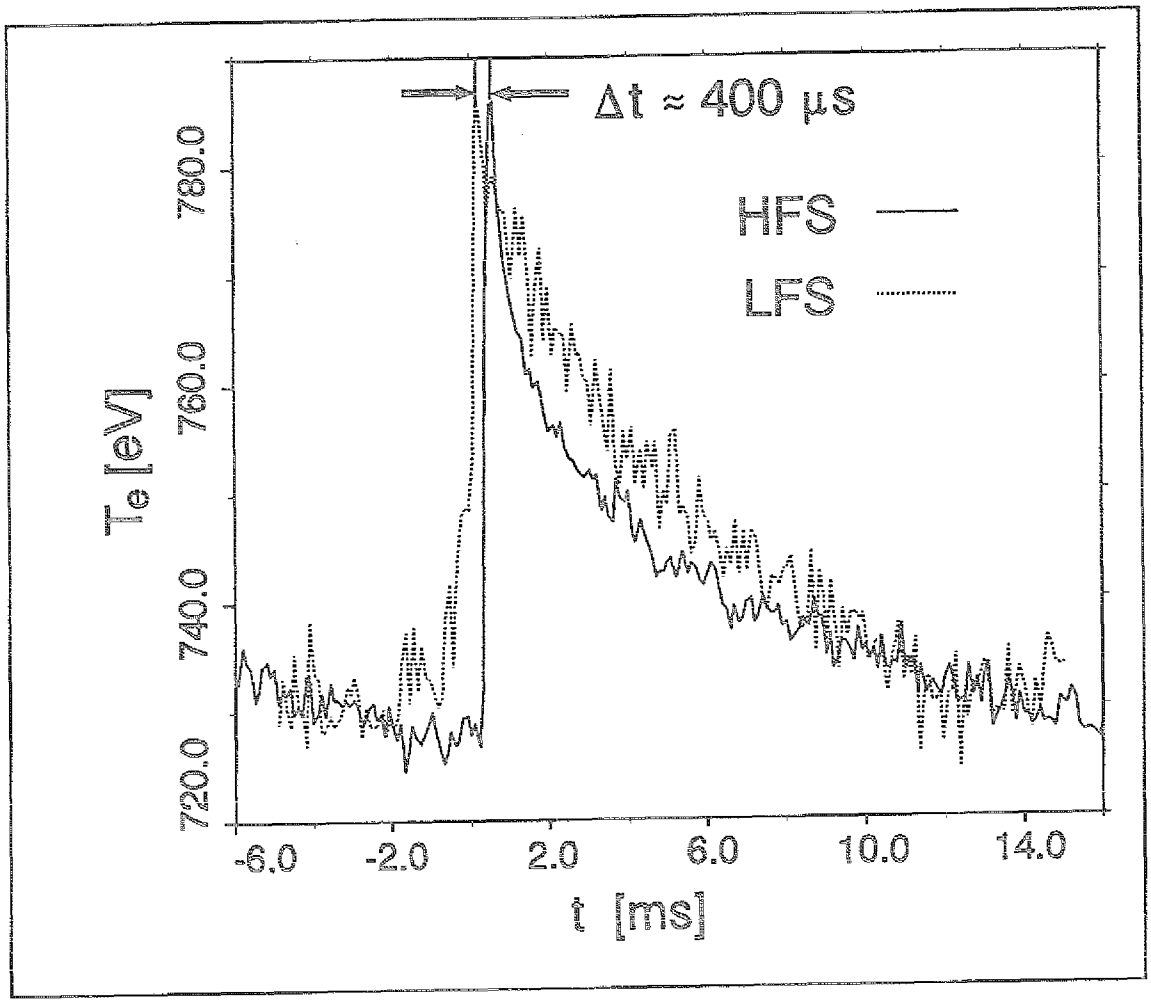
Δt ≈ 400 μs
HFS
LFS
Te [eV]
780.0
760.0
740.0
720.0
-6.0
-2.0
2.0
6.0
10.0
14.0
t [ms]

Figure 3

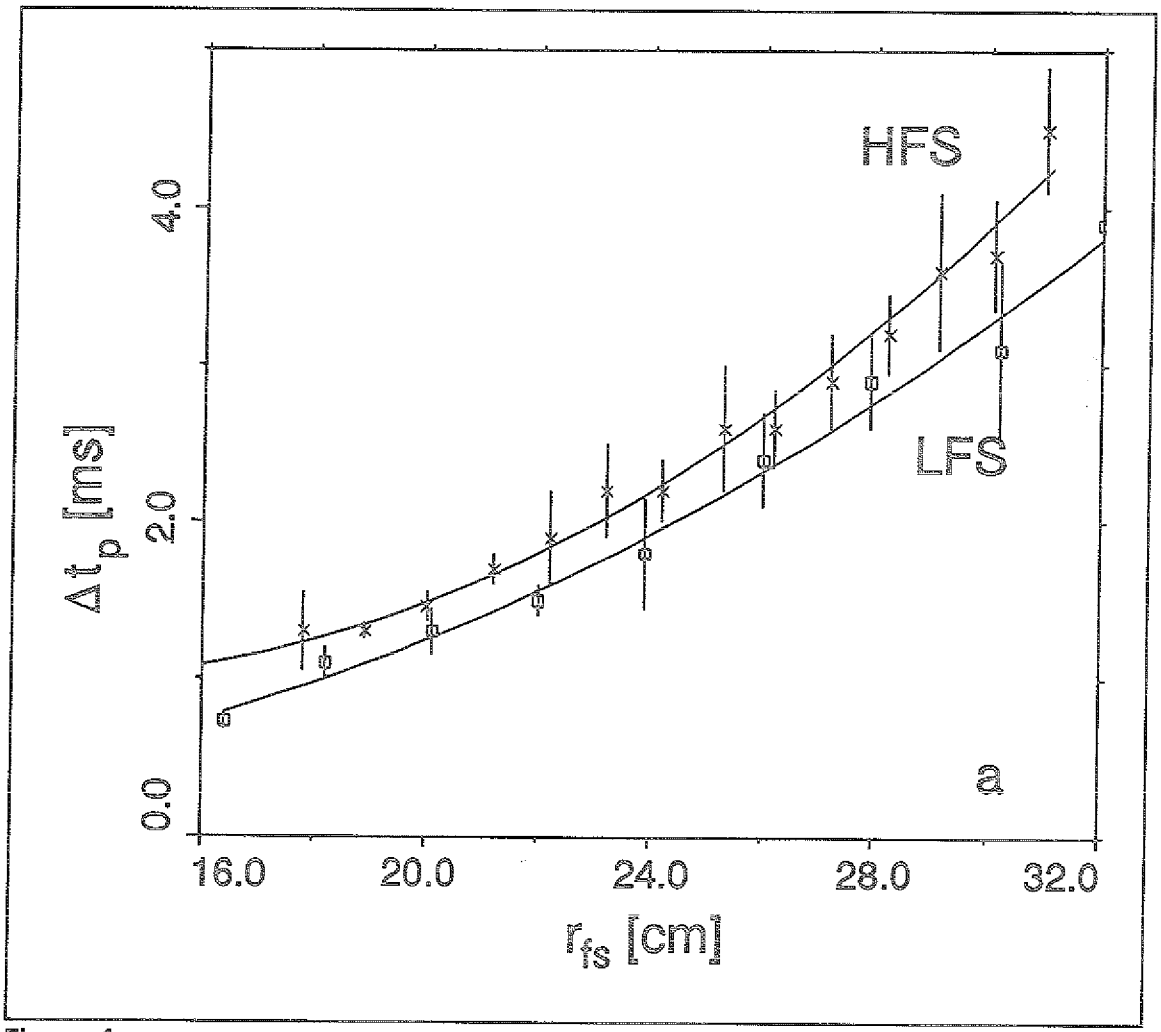

Figure 4a

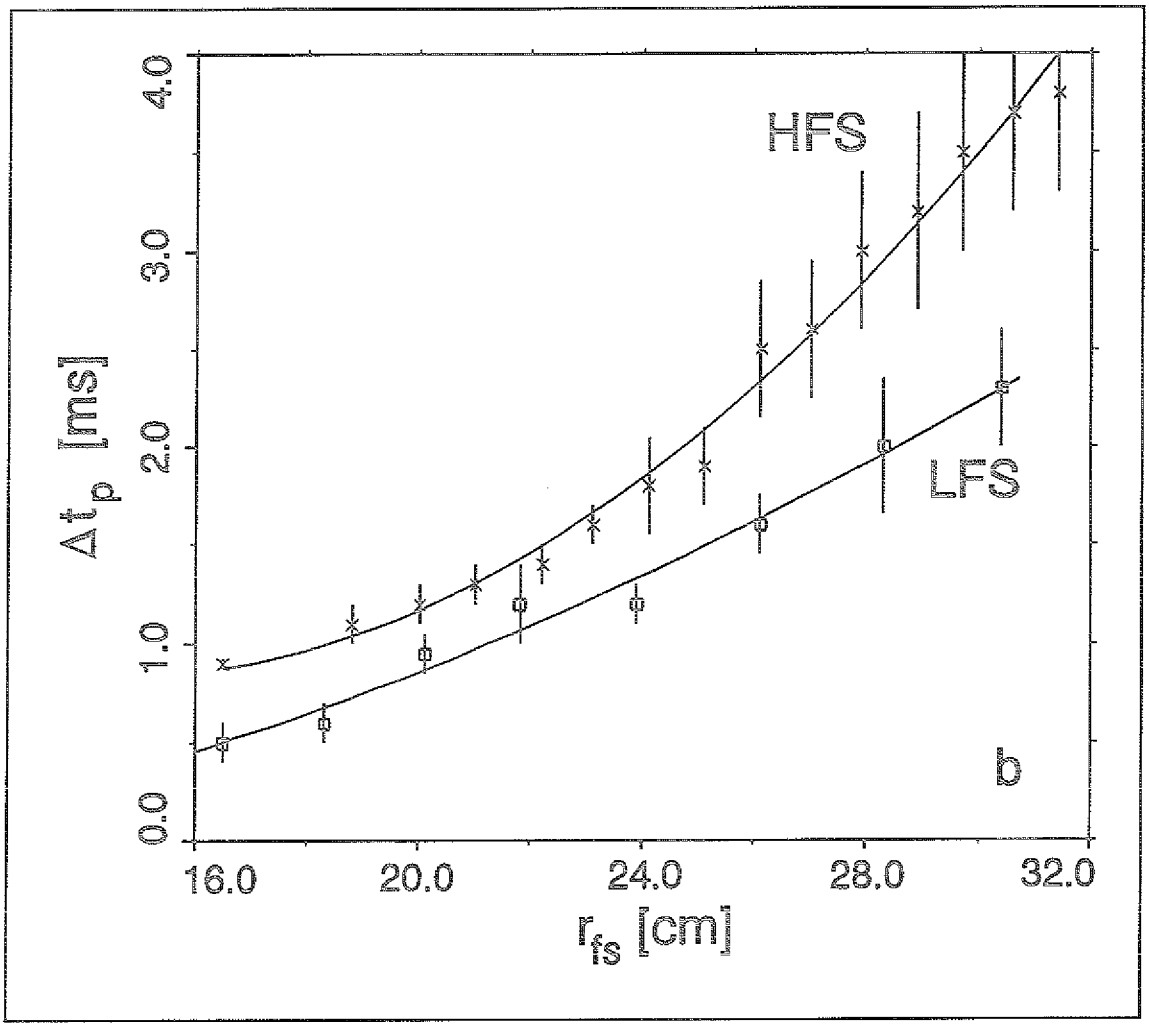

Figure 4b

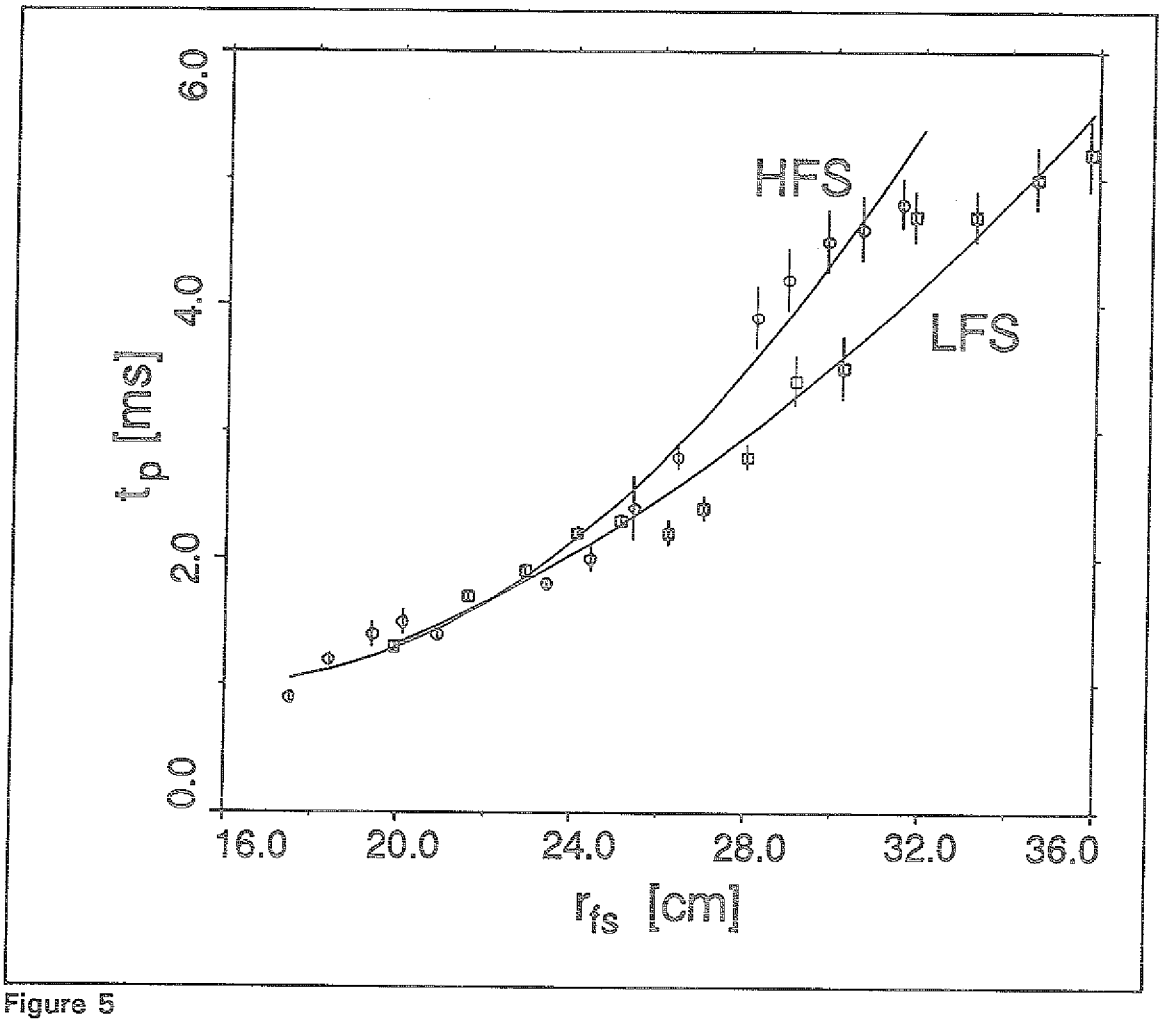

Figure 5

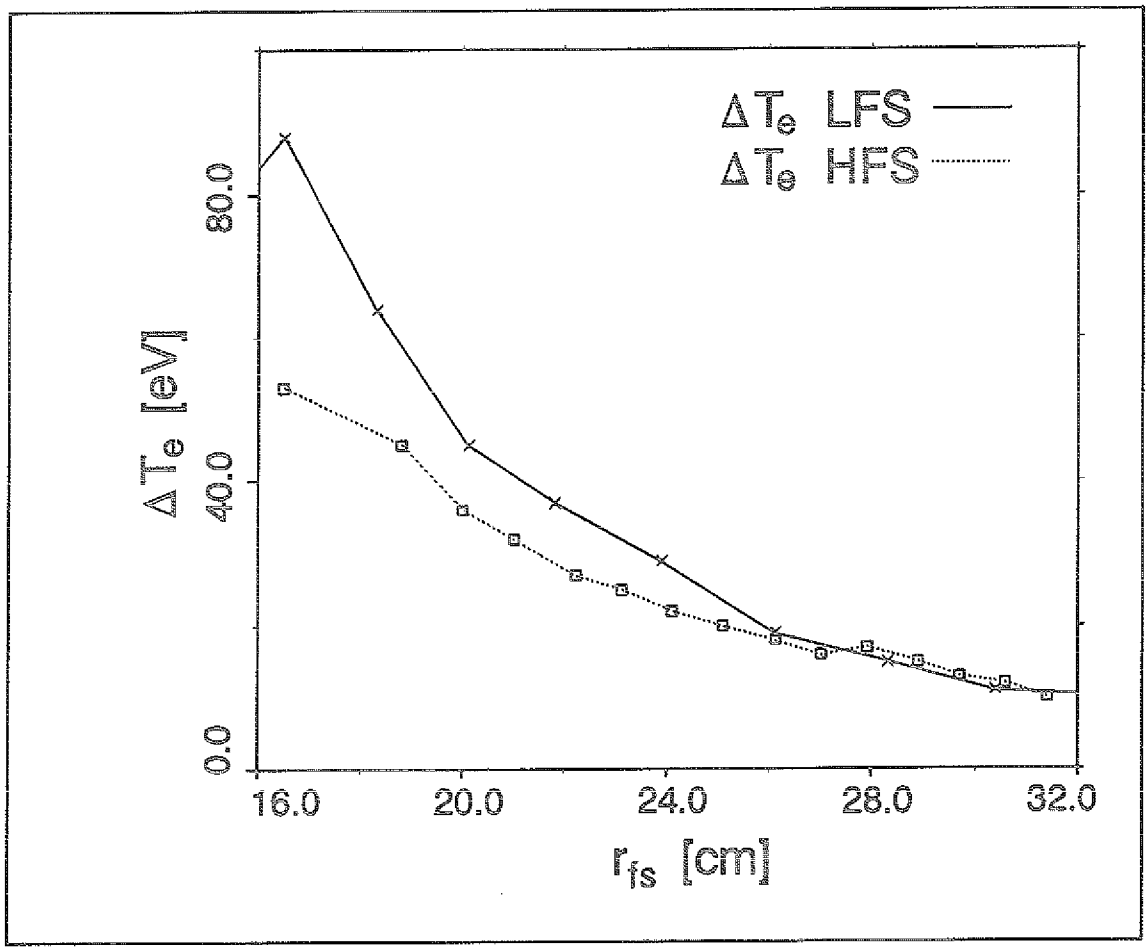

Figure 6

FORSCHUNGSZENTRUM JÜLICH GmbH

KFA

Jül-2680
October 1992
ISSN 0366-0885